

Extension of the TraPPE force field to dimethylmethyl phosphonate, sarin and soman.

Nandhini Sokkalingam, Ganesh Kamath, Maria Coscione and Jeffrey J. Potoff*

Department of Chemical Engineering and Materials Science,
Wayne State University, Detroit, MI 48202

May 26, 2009

Abstract

The Transferable Potentials for Phase Equilibria (TraPPE) force field is extended to dimethylmethylphosphonate (DMMP), sarin and soman by introducing a new interaction site representing the phosphorous atom. Parameters for the phosphorous atom are optimized to reproduce the liquid densities at 303 and 373 K and the normal boiling point of DMMP. Calculations for sarin and soman are performed in predictive mode, without further parameter optimization. Vapor-liquid coexistence curves, critical properties, vapor pressures and heats of vaporization are predicted over a wide range of temperatures with histogram reweighting Monte Carlo simulations in the grand canonical ensemble. Excellent agreement with experiment is achieved for all compounds, with unsigned errors of less than 1% for vapor pressures and normal boiling points and under 5% for heats of vaporization and liquid densities at ambient conditions.

*To whom correspondence should be addressed. E-mail: jpotoff@chem1.eng.wayne.edu. Fax 313 577 3810. Phone: 313 577 9357

1 Introduction

There has been considerable interest in the development of sensors for the detection of chemical warfare agents in the atmosphere. Promising technologies include, molecularly imprinted polymers [1, 2] or polymer composites [3], surface acoustic wave (SAW) [4], electrochemical bio-sensors [5] and metal oxide thin films and nanowires [6–10]. In addition to sensing applications, metals [11] and metal oxides [12–15] have been studied extensively as potential catalysts for the decomposition of chemical agents into non-toxic substances.

Although metal oxide based sensors exhibit high sensitivity, they suffer from poor selectivity, leading to false positives triggered by relatively innocuous materials, such as methanol. Prefiltering and concentration schemes involving physical adsorption on nanoporous silica have been proposed as a means of improving detection selectivity for chemical warfare agents [16, 17]. Due to the innate toxicity of chemical warfare agents, the majority of experimental studies are performed with relatively non-toxic simulants, such as dimethylmethylphosphonate (DMMP), which is a commonly used simulant for sarin. While the chemical adsorption of organophosphonates on metals and metal oxides is known to occur through a common mechanism of oxygen binding to the surface, much less is known about specific substrate-adsorbate interactions during physical adsorption.

Molecular simulation is well suited to the study of toxic materials, and can be used to extract information on the roles specific intermolecular interactions as long as an appropriate force field is available. Numerous *ab initio* studies have been performed to determine the optimized geometry and rotational barriers of DMMP [18–20], sarin [21] and soman [22]. Sarin interacting with metal oxide surfaces has also been studied with quantum chemical calculations [23]. Vishnyakov *et. al.* have proposed a united-atom model for DMMP [25] based on the Optimized Potentials for Liquid Simulation (OPLS) force field [24], but to date, no force fields have been reported for sarin or soman. In this work, the Transferable Potentials for Phase Equilibria (TraPPE) force field [26–37] extended to DMMP, sarin and soman, through the introduction of only two new Lennard-Jones parameters in addition to *ab initio* derived partial charge distributions. Histogram-reweighting Monte Carlo simulations in the grand canonical ensemble are used to determine the vapor-liquid coexistence curves, vapor pressures, critical points, heats of vaporization and second virial coefficients. Where appropriate, comparisons are made between the predictions given by the TraPPE and Vishnyakov force fields.

This paper is organized as follows: The force fields developed in this work are described in detail in the next section. In Section 3, the relevant details of the Monte Carlo simulations used in this work are given. In Section 4, phase diagrams, vapor pressures, heats of vaporization and critical points as predicted by the TraPPE force field are presented. The conclusions of this work can be found in Section 5.

2 Force Fields

2.1 Fluid-fluid interactions

Non-bonded interactions are given by pairwise additive Lennard-Jones (LJ) 12-6 potentials with Coulombic interactions for partial charges

$$U(r_{ij}) = 4\varepsilon_{ij} \left[\left(\frac{\sigma_{ij}}{r_{ij}} \right)^{12} - \left(\frac{\sigma_{ij}}{r_{ij}} \right)^6 \right] + \frac{q_i q_j}{4\pi\varepsilon_0 r_{ij}} \quad (1)$$

where r_{ij} , ε_{ij} , σ_{ij} , q_i , and q_j are the separation, LJ well depth, pseudo-atom diameter and partial charges, respectively, for the pair of interaction sites i and j and ε_0 is the permittivity of vacuum. A united-atom representation is used for all CH_x groups. In addition to the TraPPE force field, additional calculations are performed with a force field for DMMP developed by Vishnyakov and Neimark (VN) [25], which also uses Lennard-Jones potentials and point charges to represent interactions between interaction sites. Lennard-Jones parameters and partial charges for both force fields are listed in Table 1.

The parameters for interactions between unlike sites are determined using the Lorentz-Berthelot combining rules [38, 39].

$$\sigma_{ij} = (\sigma_{ii} + \sigma_{jj})/2 \quad (2)$$

$$\varepsilon_{ij} = \sqrt{\varepsilon_{ii}\varepsilon_{jj}} \quad (3)$$

Partial charges were generated by performing a CHELPG analysis on electrostatic potential energy surfaces determined from ab initio calculations at the HF/6-31g+(d,p) level using Gaussian 03 [40]. The Hartree Fock theory with the 6-31+g(d,p) basis set is chosen over more advanced theories, such as MP2 or B3LYP and larger basis sets because our previous calculations have shown that the HF/6-31+g(d,p) provides the best estimates of partial charges when using the CHELPG analysis [41, 42], where “best” is defined as the ability of the resulting force field to simultaneously reproduce experimental vapor pressures and saturated liquid densities. Lennard-Jones parameters for all functional groups except for P in DMMP were taken without modification from the TraPPE-UA force field [26, 28, 31, 37]. The parameters for phosphorous were tuned to reproduce the vapor pressure of DMMP over the temperature range 325-408 K and the liquid densities at 303 and 373 K according to the methodology described Ref [43]. In this case, ε for the phosphorous atom was optimized to reproduce the normal boiling point, while σ was tuned to yield the correct liquid density at 303 and 373 K. The acentric factor predicted by simulation was in close agreement with the experimental value, therefore no empirical fitting of partial charges was necessary. Calculations for sarin and soman were purely predictive, as no parameter optimization was performed in either case. Required parameters for the fluorine atom were taken from the OPLS-AA force field [44].

The TraPPE force field uses fixed bond lengths, while the VN force field uses a harmonic potential to model bond stretching

$$U_{bond} = k_{bond}(r - r_0)^2 \quad (4)$$

where k_{bond} is the force constant and r_0 is the equilibrium bond length. In both force fields a harmonic potential was used to describe bond angle bending

$$U_{bend} = \frac{k_\theta}{2}(\theta - \theta_0)^2 \quad (5)$$

where θ is the measured bond angle, θ_0 is the equilibrium bond angle and k_θ is the force constant. All the bond lengths, bond angles and the bending force constants are listed in Table 2.

Rotation about dihedral angles was controlled through a cosine series, which included a phase angle term f to account for asymmetric rotational barriers

$$U_{tors} = c_0 + c_1[1 + \cos(\phi + f)] + c_2[1 - \cos(2(\phi + f))] + c_3[1 + \cos(3(\phi + f))] \quad (6)$$

ϕ is the dihedral angle and c_i are Fourier constants, which are listed in Table 3. These coefficients were determined by fitting Equation 6 to the potential energy surfaces generated from HF/6-31g+(d,p) calculations. The conformational behavior of DMMP has been studied extensively with *ab initio* methods [18–20]. Low-energy conformers and rotational barriers for the P-O-C-C dihedral in sarin and soman have also been determined from quantum chemical calculations [21]. In this work, the focus is on developing a reliable approximation of the rotational barriers for use in the development of the TraPPE force field. Structures optimized with HF/6-31g+(d,p) compare favorably with the B3LYP results of Ref [19], predicting the lowest energy conformer for DMMP with dihedral angles of -46.93 and -24.81 degrees for the O1=P-O3-C3 and O1=P-O2-C2 dihedrals, respectively.

Energetic barriers to dihedral rotation for the O=P-O-CH₃ dihedral in DMMP and the CH₃-CH-O-P dihedral in sarin are shown in Figures 1 and 2, respectively. For DMMP, additional calculations were performed at the MP2/6-31g+(d,p) level to determine the effect of theory level on the predicted rotational barriers. As shown in Figure 1, MP2 and HF theories yield similar values for the O=P-O-CH₃ rotational barriers, which is consistent with similar calculations performed for other phosphorus containing compounds [45]. These combined results demonstrate the inclusion of electron correlation has little effect on the predicted energy minima or rotational barriers. Therefore, scanning dihedral angles with higher level theories and larger basis sets is not expected to improve the predictive capabilities for the force field.

The VN force field uses a slightly different cosine series to describe the torsional behavior

$$U_{torsion} = \sum_{i=1}^6 V_i(1 + \cos(i\phi)). \quad (7)$$

where V_i are the Fourier coefficients.

3 Simulation Details

Vapor-liquid coexistence curves, vapor pressures, heats of vaporization, and second virial coefficients were obtained from histogram reweighting Monte Carlo simulations in the grand canonical ensemble [46–48]. Insertion of molecules were enhanced through the use of the

coupled-decoupled configurational-bias Monte Carlo method [28]. 14 trial insertions were used for the first atom, and 12 trial insertions per site were used for all remaining sites. Increasing the number of attempted trial insertions beyond this was found to have a negligible effect on the fraction of accepted particle transfers. The ratios of attempted moves were set to 60% particle insertions/deletions, 10% configurational-bias regrowths, 15% translations and 15% rotations. A boxlength of 30 Å was used for DMMP and sarin while 35 Å was used for soman. Lennard-Jones interactions were truncated at 14 Å and standard long-range corrections were applied [49]. Electrostatic interactions were calculated using an Ewald sum with tin-foil boundary conditions [49, 50]. All calculations were equilibrated for 1×10^6 Monte Carlo Steps (MCS) followed by production runs of 5×10^7 MCS in the liquid phase and 1×10^7 MCS in the vapor phase. Histograms of number of particles and the energy were collected every 250 MCS during each simulation. Statistical uncertainties were determined from the standard deviation of results produced by three separate simulations started from different initial configurations and given different random number seeds.

Radial distribution functions and liquid densities at 1 atm at various temperatures were determined with *NPT* Monte Carlo simulations. Simulations were performed with 250 molecules. The ratio of moves were 1% volume changes, 14% configurational-bias regrowths, 70% translations and 15% rotations. Simulations were equilibrated for 2.5×10^7 MCS, and run statistics were recorded for an additional 2.5×10^7 MCS. All calculations in this work were performed with the Monte Carlo simulation engine MCCCS Towhee [52]

4 Results and Discussion

In the case of DMMP, sarin and soman, experimental data in the open literature are limited to liquid densities at ambient conditions, vapor pressures within 100 K of room temperature and normal boiling points [19, 53–60]. In Table 6, the predictions of the TraPPE force field for liquid densities at 1 atm and 298 K for sarin and soman, and 303 and 373 K for DMMP, are listed in comparison with experiment. The maximum deviation from experiment was found for soman, where the liquid density is over-predicted by 4.5%. For DMMP, the TraPPE force field predicts liquid densities at 303 and 373 K that are within 1% of experimental values. At these conditions, the VN force field also provides a reliable estimate of the liquid densities for DMMP.

Vapor-liquid coexistence curves predicted by the TraPPE force field are shown in Figure 3, with the predictions of the VN force field for DMMP included for comparison. The phase diagrams for sarin and soman should be considered “hypothetical,” since these compounds are known to decompose at temperatures near their normal boiling points. DMMP, sarin and soman are found to exhibit similar phase behavior, but quantitative differences are clearly apparent. Phase behavior predicted by the Vishnyakov DMMP force field differs significantly from that predicted by the TraPPE force field. This is due in part to parameterization strategy. The VN force field is built on the OPLS force field, which was developed with an emphasis in reproduction of conformational behavior and physical properties at ambient temperature and pressure. Parameters in the TraPPE force field, on the other hand, were optimized to reproduce vapor-liquid coexistence curves from ambient conditions to the critical point. As a result, TraPPE typically exhibits significantly better performance than

OPLS in the prediction of physical properties and phase behavior at conditions significantly above ambient temperature and pressure [26,37].

Experimental vapor pressures for DMMP are available for $325 \leq T \leq 408$ K and were used in the refinement of the DMMP force field. In Figure 4, Clausius-Clapeyron plots for DMMP, sarin and soman are presented along with the experimental vapor pressures. Through optimization of only the Lennard-Jones ε and σ for the P atom, in DMMP, it was possible to match closely experimental vapor pressures. Normal boiling points, listed in Table 4, were calculated for each molecule and found to be within 1.5% of experiment in all cases, which is remarkable considering that no additional parameter optimization was performed for sarin or soman. The normal boiling point for DMMP-VN was found to be 515.2 K, which is a 61.2 K over-prediction compared to experiment.

Critical temperatures and densities were computed by fitting the saturated liquid and vapor densities to the density scaling law for critical temperature [61]

$$\rho_{liq} - \rho_{vap} = B(T - T_c)^\beta \quad (8)$$

and the law of rectilinear diameters [62]

$$\frac{\rho_{liq} + \rho_{vap}}{2} = \rho_c + A(T - T_c) \quad (9)$$

where $\beta = 0.325$ is the critical exponent for Ising-type fluids in three dimensions [63] and A and B are constants fit to simulation data. The results of these calculations are listed in Table 4. Although the TraPPE and VN force fields yield similar liquid densities at 303 K, the VN force field predicts a T_c that is 100 K higher than TraPPE, illustrating how small differences in force field parameters can have large effects on predicted phase diagrams. Comparison of T_c for DMMP, sarin and soman shows DMMP with a critical temperature 70 K greater than that of sarin, while being only 25 K higher than soman's. Based on these results, DMMP is expected to provide reasonable qualitative, but not quantitative, estimates of sarin and soman phase behavior.

Heats of vaporization were calculated for each molecule as a function of temperature using histogram data collected for the vapor-liquid equilibria calculations and Equation 10

$$\Delta H_v = U_v - U_l + p(V_v - V_l) \quad (10)$$

where subscripts v and l refer to the vapor and liquid phases, respectively. U is the internal energy per mol and V is the molar volume. The results of these calculations are shown in Figure 5. Near 450 K, DMMP and soman were found to have similar heats of vaporization, while ΔH_v for sarin at 450 K was approximately 10 kJ/mol lower. Heats of vaporization predicted by the DMMP-VN force field were significantly higher than those predicted by TraPPE, which was due in large part to having a critical temperature 100 K greater than the TraPPE force field. Heats of vaporization were calculated at room temperature from NPT Monte Carlo simulations due to poor acceptance rates for the molecule insertion move in the GCMC simulations. The results of these room temperature calculations are listed in Table 5 with experimental data for comparison.

Second virial coefficients were calculated for the TraPPE force field and are listed in Table 7. The truncated virial expression is given by

$$Z = 1 + \left(\frac{B}{V}\right) \quad (11)$$

where $Z = \frac{PV}{RT}$ is the compressibility factor, B is the second virial coefficient and V is the specific volume. Histograms were reweighted for a series of chemical potentials to determine the gas phase PVT behavior of the compounds at 450, 550, and 650 K. The resulting data were plotted as $Z - 1$ vs $1/V$, and the second virial coefficients were determined by taking the slope of the regression line fit to data. The magnitude of the second virial coefficients, especially near the normal boiling point, illustrates non-ideal behavior in the gas phase.

NPT Monte Carlo simulations were used to investigate the liquid phase structure of the TraPPE and VN force fields for DMMP at 303 K and 1.01 bar. Radial distribution functions for various interactions are shown in Figure 6 and a schematic of DMMP is presented in Figure 7 for reference. Both force fields provided similar results for the C3-C3 and C1-O2 interactions, while significant differences were observed in the O1-C1 interaction. The VN force field predicted a slightly more ordered liquid phase, where DMMP molecules were able to orient themselves to create O1-C1 nearest neighbor interactions. The difference in the O1-C1 RDF predicted by the VN and TraPPE force field was likely due to differences in the bonded interactions, which in the case of the TraPPE force field sterically hinder the formation of O1-C1 nearest neighbor pairs. In the absence of experimental x-ray or neutron scattering data, however, it is not possible to determine which force field provides a more accurate picture of microscopic structure in DMMP.

5 Conclusion

The TraPPE force field has been extended to DMMP, sarin and soman. Excellent reproduction of limited experimental data was achieved through the introduction of two additional parameters; the Lennard-Jones σ and ε for the phosphorous atom in DMMP. Calculations for sarin and soman were performed in predictive mode, and yielded liquid densities and normal boiling points within 1% of experiment. The force field for DMMP is a significant improvement over existing force fields, especially with respect to the reproduction of normal boiling points and vapor pressures, making it especially useful for the simulation of adsorption isotherms. Hypothetical vapor-liquid coexistence curves and critical parameters calculated in this work are expected to be of use for equation of state modeling of these compounds, which generally rely on knowledge of the critical properties and acentric factor. The force fields themselves may be used to study a wide range of topics involving transport, adsorption and partitioning of chemical agents.

6 Acknowledgments

The authors wish to thank Alex Balboa and Guy Cabel for useful discussions. Part of the computer resources used in this work were provided by Grid Computing at Wayne State University. Funding from NSF-CBET-0522005 is gratefully acknowledged.

7 Supporting Information

Tabulated numerical data for all results presented in this work are available free of charge via the Internet at <http://pubs.acs.org>.

References

- [1] Zhou, T.; Yu, B.; Shiu, E.; Levon, K. *Anal. Chem.* **2004**, *76*, 2689.
- [2] Prathish, K. P.; Prasad, K.; Prasada Rao, T. Suryanarayana, M. V. S. *Talanta*, **2007**, *71*, 1976.
- [3] Hopkins, A. R.; Lewis, N. S. *Anal. Chem.*, **2001**, *73*, 884.
- [4] Du, X.; Ying, Z.; Jiang, Y.; Liu, Z.; Yang, T.; Xie, G. *Sens. and Actuators B: Chemical* **2008**, *134*, 409.
- [5] Arduini, F.; Amine, A.; Moscone, D.; Ricci, F.; Palleschi, G. *Anal. Bioanal. Chem.* **2007**, *388*, 1049.
- [6] Oh, S. W.; Kim, Y. H.; Yoo, D. J.; Oh, S. M.; Park, S. J. *Sens. Actuators B* **1993**, *13/14*, 400.
- [7] Tomchenko, A. A.; Harmer, G. P.; Marquis, B. T. *Sens. Actuators B* **2005**, *108*, 41.
- [8] Brunol, E.; Berger, F.; Fromm, M.; Planade, R. *Sens. Actuators B* **2006**, *120*, 35.
- [9] Zuo, G.; Li, X.; Li, P.; Yang, T.; Wang, Y.; Cheng, Z.; Feng, S. *Analytica Chimica Acta* **2006**, *580*, 123.
- [10] Ponzoni, A.; Baratto, C.; Bianchi, S.; Comini, E.; Ferroni, M.; Pardo, M.; Vezzoli, M.; Vomiero, A.; Faglia, G.; Sberverglieri, G. *IEEE Sensors Journal* **2008**, *8*, 735.
- [11] Guo, X.; Yoshinobu, J.; Yates Jr., J. T. *J. Phys. Chem.* **94**, 6839, (1990).
- [12] Templeton, M. K.; Weinberg, W. H. *J. Amer. Chem. Soc.* **1985**, *107*, 97.
- [13] Mitchell, M. B.; Sheinker, V. N.; Mintz, E. A. *J. Phys. Chem. B* **1997**, *101*, 11192.
- [14] Rusu, C. N.; Yates Jr., J. T. *J. Phys. Chem. B* **2000**, *104*, 12292.
- [15] Kim, C. S.; Lad, R. J.; Tripp, C. P. *Sens and Actuators B* **2001**, 442.
- [16] Kanan, S. M.; Tripp, C. P. *Langmuir* **2001**, 2213.
- [17] Kanan, S. M.; Tripp, C. P. *Langmuir* **2002**, 722.
- [18] Ault, B. S.; Balboa, A.; Tevault, D.; Hurley, M. *J. Phys. Chem. A* **2004**, *108*, 10094.

- [19] Cuisset, A.; Mouret, G.; Pirali, O.; Roy, P.; Cazier, F.; Nouali, H.; Demaison, J. *J. Phys. Chem. B* **2008**, *112*, 12516.
- [20] Suenram, R. D.; Lovas, F.J.; Plusquellic, D. F.; Lesarri, A.; Kawashima, Y.; Jensen, J. O.; Samuels, A. C. **2002**, *211*, 110.
- [21] Kaczmarek, A.; Gorb, L.; Sadlej, A. J.; Leszczynski, J. *Structural Chemistry* **2004**, *15*, 517.
- [22] Majumdar, D.; Roszak, S.; Leszczynski, J. *Mol. Phys.* **2007**, *105*, 2551.
- [23] Michalkova, A.; Gorb, L.; Ilchenko, M.; Zhikol, O. A.; Shishkin, O. V.; Leszczynski, J. *J. Phys. Chem. B*, **2004**, *15*, 1918.
- [24] Kaminski, G.; Duffy, E. M.; Matsui, T.; Jorgensen, W. L. *J. Phys. Chem.* **1994**, *98*, 13007.
- [25] Vishnyakov, A.; Neimark, A. V. *J. Phys. Chem. A* **2004**, *108*, 1435.
- [26] Martin M. G.; Siepmann, J. I. *J. Phys. Chem. B* **1998**, *102*, 2569.
- [27] Chen, B.; Siepmann, J. I. *J. Phys. Chem. B* **1999**, *103*, 5370.
- [28] Martin M. G.; Siepmann, J. I. *J. Phys. Chem. B* **1999**, *103*, 4508.
- [29] Wick, C. D.; Martin, M. G.; Siepmann, J. I. *J. Phys. Chem. B* **2000** *104*, 8008.
- [30] Chen, B.; Potoff, J. J.; Siepmann, J. I. *J. Phys. Chem. B* **2001**, *105*, 3093.
- [31] Stubbs, J. M.; Potoff, J. J.; Siepmann, J. I. *J. Phys. Chem. B* **2004**, *108*, 17596.
- [32] Wick, C. D.; Stubbs, J. M.; Rai, N.; Siepmann, J. I. *J. Phys. Chem. B* **2005**, *109*, 18974.
- [33] Lubna, N.; Kamath, G.; Potoff, J. J.; Rai, N.; Siepmann, J. I. *J. Phys. Chem. B* **109**, 24100.
- [34] Rai, N.; Siepmann, J. I. *J. Phys. Chem. B* **2007**, *111*, 10790.
- [35] Potoff, J. J.; Siepmann, J. I. *AICHE J.*, **2001**, 1676.
- [36] Zhang, L.; Siepmann, J. I. *J. Phys. Chem. B* **2005**, *109*, 2911.
- [37] Kamath, G.; Cao, F.; Potoff, J.J. *J. Phys. Chem. B* **2004**, *108*, 14130.
- [38] Lorentz, H. A. *Ann. Phys.* **1881**, *12*, 127.
- [39] Berthelot, D. C. *R. Hebd. Seanc. Acad. Sci. (Paris)* **1898**, *126*, 1703.

- [40] Gaussian 03, Revision A.1 , Frisch, M. J.; Trucks, G. W.; Schlegel, H. B.; Scuseria, G. E.; Robb, M. A.; Cheeseman, J. R.; Montgomery, Jr., J. A.; Vreven, Englewood Cliffs, NJ, T.; Kudin, K. N.; Burant, J. C.; Millam, J. M.; Iyengar, S. S.; Tomasi, J.; Barone, V.; Mennucci, B.; Cossi, M.; Scalmani, G.; Rega, N.; Petersson, G. A.; Nakatsuji, H.; Hada, M.; Ehara, M.; Toyota, K.; Fukuda, R.; Hasegawa, J.; Ishida, M.; Nakajima, T.; Honda, Y.; Kitao, O.; Nakai, H.; Klene, M.; Li, X.; Knox, J. E.; Hratchian, H. P.; Cross, J. B.; Adamo, C.; Jaramillo, J.; Gomperts, R.; Stratmann, R. E.; Yazyev, O.; Austin, A. J.; Cammi, R.; Pomelli, C.; Ochterski, J. W.; Ayala, P. Y.; Morokuma, K.; Voth, G. A.; Salvador, P.; Dannenberg, J. J.; Zakrzewski, V. G.; Dapprich, S.; Daniels, A. D.; Strain, M. C.; Farkas, O.; Malick, D. K.; Rabuck, A. D.; Raghavachari, K.; Foresman, J. B.; Ortiz, J. V.; Cui, Q.; Baboul, A. G.; Clifford, S.; Cioslowski, J.; Stefanov, B. B.; Liu, G.; Liashenko, A.; Piskorz, P.; Komaromi, I.; Martin, R. L.; Fox, D. J.; Keith, T.; Al-Laham, M. A.; Peng, C. Y.; Nanayakkara, A.; Challacombe, M.; Gill, P. M. W.; Johnson, B.; Chen, W.; Wong, M. W.; Gonzalez, C.; and Pople, J. A.; Gaussian, Inc., Pittsburgh PA, 2003.
- [41] Kamath, G.; Lubna, N.; Potoff, J. J. *J. Chem. Phys.* **2005**, *123*, 124505.
- [42] Ketko, M. H.; Potoff, J. J. *Mol. Sim.* **2007**, *33*, 769.
- [43] Ketko, M. H.; Rafferty, J.; Siepmann, J. I.; Potoff, J. J. *Fluid Phase Equil.* **2008**, *274*, 44.
- [44] Watkins, E. K.; Jorgensen, W. L. *J. Phys. Chem A* **2001**, *105*, 4118.
- [45] Stewart, E. L.; Norman, N. N.; Allinger, N. L.; Bowen, J. P. *J. Org. Chem.* **1997**, *62*, 5198.
- [46] Ferrenberg, A. M.; Swendsen, R. H. *Phys. Rev. Lett.* **1988**, *61*, 2635.
- [47] Ferrenberg, A. M.; Swendsen, R. H. *Phys. Rev. Lett.* **1989**, *63*, 1195.
- [48] Potoff, J. J.; Panagiotopoulos, A.Z. *J. Chem. Phys.* **1998**, *109*, 10914.
- [49] Allen, M. P. and Tildesley, D. J. *Computer Simulation of Liquids*, 1st edition, (Clarendon Press, Oxford, 1987).
- [50] Ewald, P. P. *Ann. Phys.* **1921**, *64*, 253.
- [51] Panagiotopoulos, A. *Mol. Phys.* **1987**, *62*, 701.
- [52] Martin, M. G.; <http://towhee.sourceforge.net/>
- [53] Tevault, D. E.; Buchanan, J. H.; Buettner, L. C. *Int. J. Thermophys.* **2006**, *27*, 486.
- [54] Butrow, A. B.; Buchanan, J. H.; Tevault, D. E.; *J. Chem. Eng. Data* **ASAP 2009**.
- [55] Belkin, F.; Brown, Jr., H. A. *Vapor Pressure Measurements of Some Chemical Agents using Differential Thermal Analysis. Part III* **1975**, EC-TR-75032; Edgewood Arsenal: Edgewood, MD, UNCLASSIFIED Report (AD-A010 666).

- [56] Buchanan, J. H.; Sumpter, K. B.; Abercrombie, P. L.; Tevault, D. E. *Vapor Pressure of GB* **2009**, ECBC-TR-xyz; Edgewood, MD, UNCLASSIFIED Report (HP-5890 GC).
- [57] Kosolapoff, G.M. *J. Chem. Soc.* **1955**, 2964.
- [58] Tevault, D. E.; Keller, J.; Parson J.; ERDEC U.S Army Technical Report.
- [59] Kosolapoff, G. M. *J. Chem. Soc.* **1954**, 3222.
- [60] Kosolapoff, G. M. *J. Am. Chem. Soc.* **1954**, *76*, 615.
- [61] J. S. Rowlinson and B. Widom, / *Molecular Theory of Capillarity* (Clarendon Press, Oxford, 1982).
- [62] J.S. Rowlinson and F.L. Swinton, *Liquids and Liquid Mixtures*, 3rd edn. (Butterworth, London, 1982).
- [63] Privman, V.; Trigg, G. L. *Encyclopedia of Applied Physics* **vol.23**, Wiley-VCH, Berlin (1998), p.41.
- [64] Langford, R. E. *Introduction to Weapons of Mass Destruction- Radiological, Chemical and Biological* **2004**, John Wiley & Sons, New Jersey.

Table 1: Parameters for non-bonded interactions Parentheses denote functional group attached to the atom of interest.

DMMP	ε [K]	σ [Å]	q [e]
CH ₃	98.0	3.75	0.28 ^a / -0.14 ^b
O-(CH ₃)	55.0	2.80	-0.53
O=(P)	79.0	3.05	-0.80
P	86.0	4.00	1.44
Sarin			
CH ₃	98.0	3.75	-0.10 ^b / -0.08 ^c
CH-(O)	10.0	4.68	0.62
O-(CH)	55.0	2.80	-0.63
O=(P)	79.0	3.05	-0.77
P	86.0	4.00	1.40
F	26.7	2.95	-0.34
Soman			
CH ₃	98.0	3.75	-0.08 ^b / -0.10 ^c / -0.15 ^d
CH	10.0	4.33	0.43
C	0.5	6.40	0.54
O-(CH)	55.0	2.80	-0.63
O=(P)	79.0	3.05	-0.77
P	86.0	4.00	1.40
F	26.7	2.95	-0.34
DMMP-VN			
CH ₃	104.04	3.80	0.131 ^a / -0.021 ^b
O-(CH ₃)	80.23	3.03	-0.36
O=(P)	80.23	2.93	-0.691
P	174.5	3.83	1.17

^a Site adjacent to oxygen. ^b Site adjacent to phosphorous.

^c Site adjacent to CH group. ^d Site adjacent to C.

Table 2: Vibration and bending parameters for DMMP, sarin and soman.

Vibration	Bond length [Å]	Bending	Bond angle [deg]	k_θ/k_b [K]
P=O	1.458	\angle O=P-CH ₃	116.3	80586
P-CH ₃	1.79	\angle O=P-O	116.5	100794
P-O	1.58	\angle CH ₃ -P-O	104.3	40894
O-CH ₃	1.41	\angle CH ₃ -O-P	121	80586
CH ₃ -CH	1.54	\angle O-P-O	106.5	62500
CH-O	1.41	\angle CH ₃ -CH-O	106.0	62500
CH-C	1.54	\angle CH ₃ -CH-CH ₃	114	62500
CH ₃ -C	1.54	\angle CH ₃ -C-CH ₃	109.4	62500
F-P	1.58	\angle CH ₃ -P-F	104.3	40894

Table 3: Torsional parameters for DMMP, sarin and soman.

Dihedral	c_0	c_1	c_2	c_3	f
O=P-O-CH ₃	1534.91	-1102.11	291.88	397.57	-0.15
CH ₃ -CH-O-P	1041.22	-753.00	432.00	227.00	1.88
CH ₃ -P-O-CH	57.48	1476.00	184.10	0.00	-0.34
O=P-O-CH	2996.00	-1467.00	215.00	-31.60	0.44
CH ₃ -C-CH-O	0.00	176.60	-53.30	769.90	0.00
CH ₃ -C-CH-CH ₃	0.00	355.00	-68.20	791.30	0.00

Table 4: Predicted critical parameters and normal boiling points for DMMP, sarin and soman.

Compound	T_c (K)	P_c (bar)	ρ_c (kg/m ³)	T_b (K)	Expt T_b (K)	ω
DMMP	700.6±0.1	49.7±0.1	368.8±0.1	458.4±0.2	453.8 [54]	0.39
DMMP-VN	801.1±0.2	52.1±0.1	360.7±0.2	515.2±0.8	453.5 [54]	0.32
Sarin	629.8±0.9	36.1±0.1	355.4±0.1	427.0±0.3	431 [64]	0.40
Soman	674.9±0.3	29.2±0.1	332.0±0.3	467.6±0.6	471 [64]	0.41

Table 5: Predicted heats of vaporization for DMMP, sarin and soman.

Compound	Temp(K)	Sim (kJ/mol)	Expt (kJ/mol)
DMMP	303	54.27±0.7	52.25 [59, 60]
DMMP (VN)	303	50.11 [25]	
Sarin	298	49.50±0.5	46.89 [64]
Soman	298	53.93±0.3	55.18 [64]

Table 6: Liquid densities predicted for DMMP, sarin and soman.

Compound	ρ_l (kg/m ³)	Expt ρ_l (kg/m ³)
DMMP (303 K)	1145.6, [1156.2] ^a	1150.7 [59]
DMMP (373 K)	1078.0, [1085.3] ^a	1071.7 [60]
Sarin (298 K)	1123.4	1088.7 [64]
Soman (298 K)	1067	1022 [64]

^a Predictions of the VN force field.

Table 7: Second virial coefficients for DMMP, sarin and soman. Units are cm^3/mol .

T (K)	650	550	450
DMMP	-455.05	-785.44	-1524.00
Sarin	-424.81	-699.19	-1363.7
Soman	-641.70	-1116.70	-2177.30

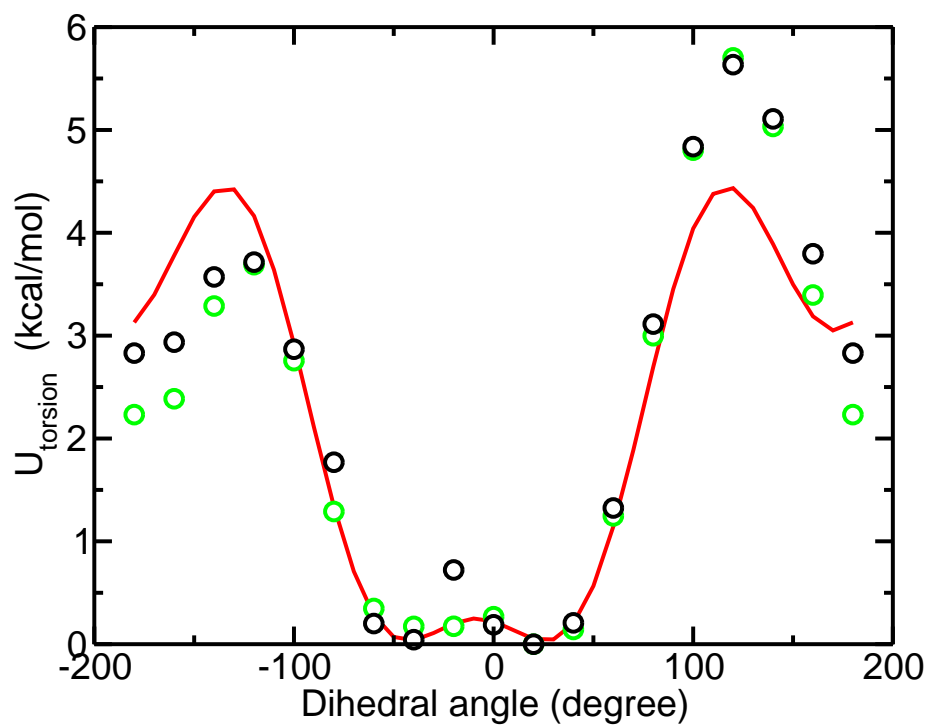


Figure 1: Torsional barrier for O=P-O-CH₃ dihedral in DMMP. Prediction of HF/6-31g+(d,p) calculations (black), MP2/6-31g+(d,p) (green) and fit of Equation 6 to data (line).

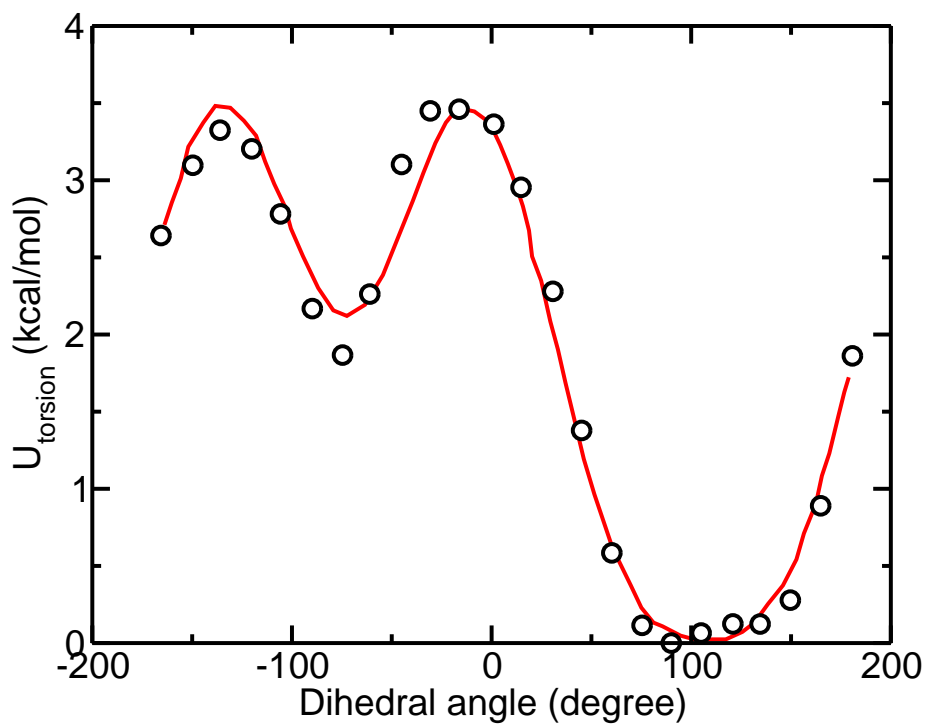


Figure 2: Torsional barrier for $\text{CH}_3\text{-CH-O-P}$ dihedral in sarin. Circles represent the results of HF/6-31g+(g,p) *ab initio* calculations, while a solid line is used to represent the fit of Equation 6 to the *ab initio* data.

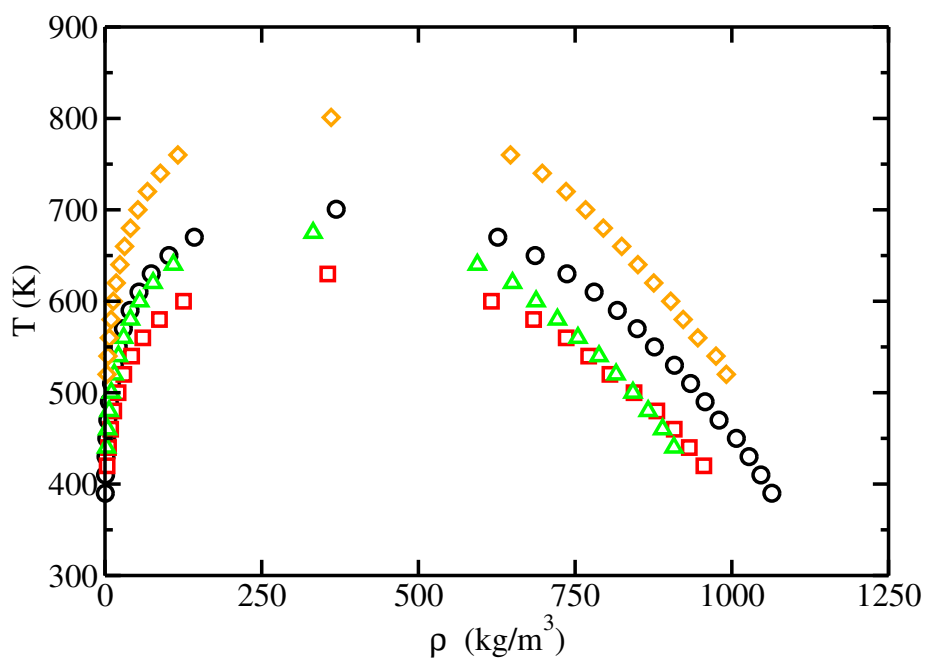


Figure 3: Vapor Liquid Equilibria for pure DMMP (circle), DMMP-VN (diamond), sarin (square) and soman (triangle).

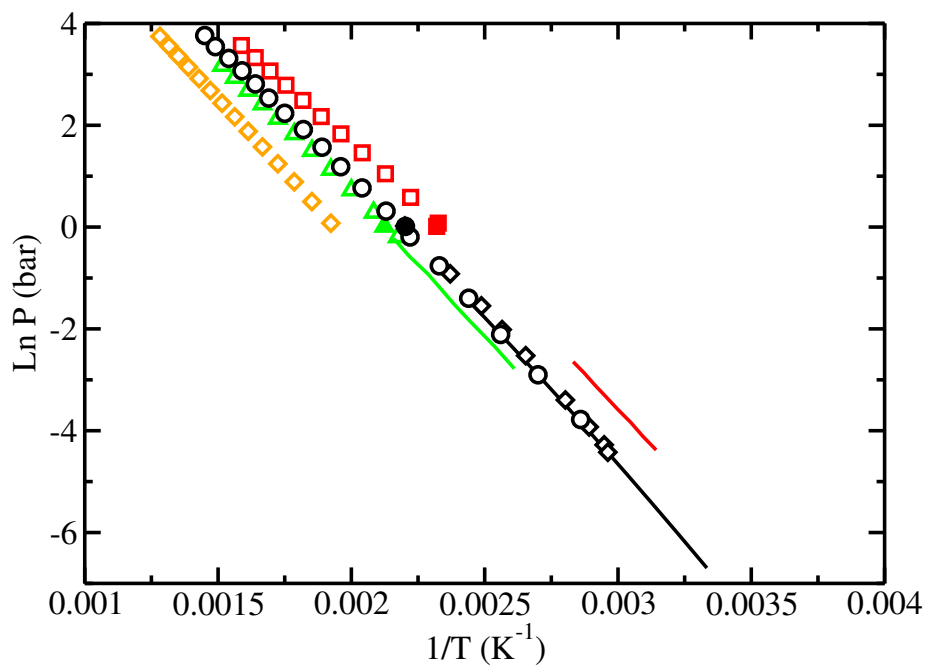


Figure 4: Clausius-Clapeyron plot for pure DMMP (circle), DMMP-VN (diamond), sarin (square) and soman (triangle). Line represents the experimental vapor pressure of pure DMMP (black) [57, 58], sarin (red) [56] and soman (green) [55]. Filled symbols represent experimental boiling points [57, 64]. Black diamonds correspond to a recently published set of experimental vapor pressure data for DMMP [54].

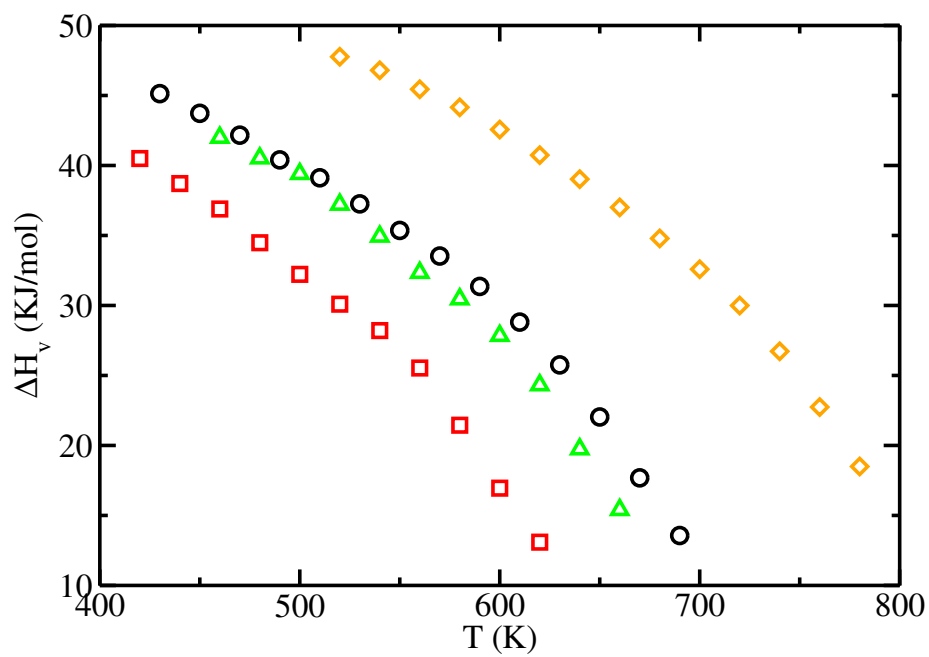


Figure 5: Heat of vaporization for DMMP (circle), DMMP-VN (diamond), Sarin (square) and soman (triangle).

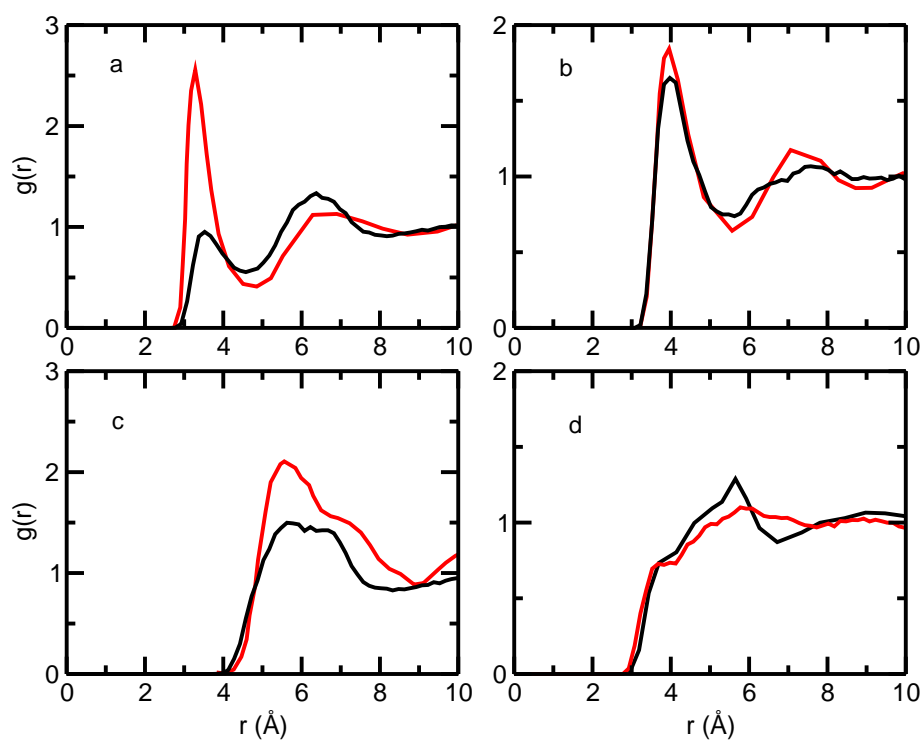


Figure 6: Radial distribution function for liquid DMMP at 303 K. New force field (black) and VN force field (red). a)O1-C1 b)C3-C3 c)P-P d)C1-O2.

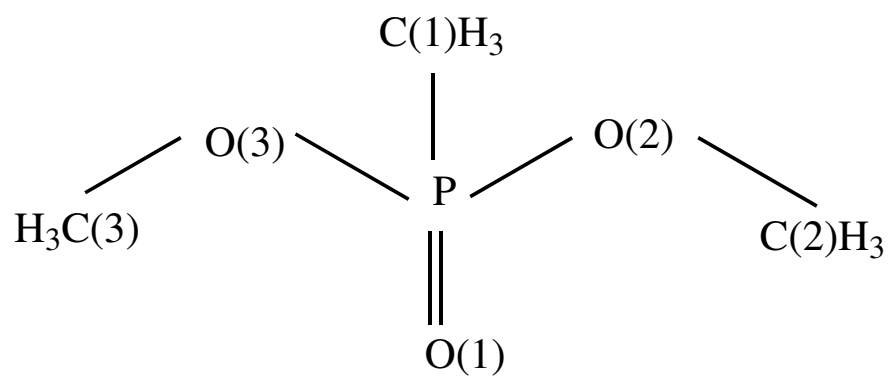


Figure 7: Schematic of DMMP